FerryBox-assisted monitoring of mixed layer pH in the Norwegian Coastal Current

Emanuele R. Reggiani[1,*], Andrew L. King[1,*], Marit Norli[2], Pierre Jaccard[2], Kai Sørensen[2], Richard G. J. Bellerby[1,3]

[1]Norwegian Institute for Water Research (NIVA), Thormøhlensgate 53D, NO-5006, Bergen, Norway
[2]Norwegian Institute for Water Research (NIVA), Gaustadalléen 21, NO-0349, Oslo, Norway
[3]State Key Laboratory for Estuarine and Coastal Research, East China Normal University, Zhongshan N. Road, 3663, Shanghai 200062, China

*corresponding authors: andrew.king@niva.no; emanuele.roberto.reggiani@niva.no

Keywords: pH; carbonate chemistry; ocean acidification; FerryBox; underway monitoring; spectrophotometry

Highlights:

- Automated, flow-through, spectrophotometric pH detector developed for FerryBox platforms
- *In situ* uncertainty <0.0003 and compliant with best practices
- Norwegian Coastal Current wintertime pH relatively low and stable
- Spring and summertime pH higher and more variable, coincident with higher chlorophyll

Abstract

The evaluation of marine carbonate system variability and the impacts of ocean acidification (OA) on coastal marine ecosystems increasingly rely on monitoring platforms capable of delivering near real-time *in situ* carbonate system observations. These observations are also used for developing models and scenarios of OA, including potential impacts on marine ecosystem structure and function. An embedded flow-through spectrophotometric pH detection system has been developed alongside an underway seawater sampling system - termed a FerryBox - operating on ships of opportunity (SOOP), and can deliver a continuous data stream of mixed layer seawater pH with an *in situ* uncertainty of <0.003. We report metrological approaches behind the pH detection procedure and the evaluation of dye addition perturbation with analytical precision as low as 0.0005. In addition, we present field-based observations from a deployment of the pH detection system along the Norwegian Coastal Current in winter, spring, and summer periods of 2015. Spring and summertime pH was generally ~0.1 higher, and up to ~0.255 higher, in comparison to winter pH observations. Here we show the necessity for a regular, high density monitoring approach, and the suitability of this pH detection technique for unmanned observational platforms.

1. INTRODUCTION

The oceans have been recognized as an important sink of CO_2 emissions from anthropogenic sources (e.g., Doney et al., 2009; Sabine et al., 2004). This is in large part due to time series observations and models for estimating ocean-atmosphere interactions. Dissolved CO_2 in the ocean's surface produces carbonic acid that dissociates releasing hydrogen ions. The net result of CO_2 uptake is an increase in hydrogen ion concentration - hence a decrease in pH - commonly referred to as ocean acidification (OA) (Doney et al., 2009).

The need for understanding the changing chemistry of the ocean and the impacts of OA on marine ecosystems has catalysed the development of platforms and technologies capable of observing the marine carbonate system at suitable space-time resolution. Coastal regions, in particular, present a challenging environment for carbonate system observations due to processes including, but not limited to, freshwater input, mixing and transport, interaction with shelf geochemistry, and large seasonal algal blooms. Gathering the required field data using conventional sampling efforts (i.e., research cruises) is demanding in terms of costs and logistics, and, due to relatively poor spatial and temporal coverage, do not have the required resolution for observing high frequency or regionally-specific variability (Hofmann et al., 2011; McNeil and Sasse, 2016). Recent efforts have shown great promise in reducing these costs by taking advantage of ships of opportunity (SOOP), container or passenger ships that regularly operate along transects, as mobile platforms for oceanic data collection using pump and sensor packages called FerryBoxes (Petersen, 2014). These systems can collect oceanographic and atmospheric data from physical, biogeochemical, and meteorological sensors coupled with GPS information, and in some cases provide satellite-based ship to shore data transfer.

The commercial availability of instruments for measuring the seawater carbonate system variables - partial pressure of carbon dioxide (pCO_2), pH, total alkalinity (AT), and total dissolved inorganic carbon (CT) - is a testament of the maturity of technology for underway and autonomous OA observations (Martz et al., 2015). In the case of AT and CT, reliable and high quality measurements still rely on benchtop set-ups for fulfilling "climate" level analytical figures of merit (Newton et al. 2014). In terms of autonomous carbonate system observations, a promising approach comes from simultaneous spectrophotometric detection of CT and pH, in which a three-week time-series deployment of an autonomous system achieved ~4 µmol kg^{-1} and 0.0025 accuracy, respectively (Wang et al., 2015).

The development of systems for unattended spectrophotometric measurement of pH using an indicator dye, both for ship-based continuous underway measurements and autonomous *in situ* devices, has indeed received renewed interest during last two decades for improved schemes based on the cost effectiveness of miniaturized spectrophotometers, mini-fluidic techniques, and embedded systems (for underway: Aβmann et al., 2011; Bellerby et al., 2002; DelValls, 1999; Mosley et al., 2004; Ohline et al., 2007; Reggiani et al., 2014; Rérolle et al., 2013; Tapp et al., 2000; Wang et al., 2007; Yang et al., 2014; and for *in situ*: Kaltenbacher et al., 2000; Liu et al., 2006; Martz et al., 2003; Nakano et al., 2006; Seidel et al., 2008). Spectrophotometric techniques have the unique advantage that no calibration is required for evaluation of pH on total scale, as long as the behaviour of a specific indicator in seawater has been characterized in terms of absorbance and protonation and then reported to measurement conditions. Major differences between the above-mentioned spectrophotometric pH systems include the pathlength through which light absorption is measured, the light source (tungsten, light emitting diode, etc.), modes of mixing sample and reagents (mixing coil, stir bar, etc.),

temperature at which measurements are made (controlled or *in situ*), and sample analysis time (including performing blank and dye perturbation measurements).

In this article, we discuss the development of a flow-through, spectrophotometric, underway pH detection instrument coupled to a FerryBox system that has been previously described in Reggiani et al. (2014). The system has been custom-designed to address several factors: resistance to biofouling, a sampling rate high enough to follow the highly dynamic coastal environment, analytical resolution better than 0.001, long-term stability, ease of installation and operation by untrained personnel, low power and low cost, open-source architecture for future development, and integration with unmanned surface vehicles. The principle of operation will be described with emphasis on methods used to provide the accuracy required to meet the "weather" and the "climate" achievements: the former indicates the capability to identify relative spatial patterns and short-term variations underlying impacts on local, immediate dynamics of ocean acidification, the latter high confidence level measurements capable to assess long-term trends (multi-decadal time scales) in order to detect anthropogenic driven changes on carbon chemistry (Newton et al., 2014). Observational data including temperature, salinity, chlorophyll a fluorescence, and pH from five cruises along the Norwegian coast between winter and summer of 2015 will also be presented.

2. MATERIALS AND METHODS

2.1. *The spectrophotometric pH detection system*

The pH detection scheme is based on the embedded-spectrophotometry flow-through system described in Bellerby et al. (2002) and modified as described in Reggiani et al. (2014) (Fig. 1). A detailed description of the standalone detection system is presented in Reggiani et al. (2014). Briefly, the pH sensor relies on water flow generated by the main FerryBox peristaltic pump that delivers a continuous flow of seawater from an inlet pipe that is situated at ~3-5 meters depth and provides seawater directly from the other side of the ship's hull. The flow-through set-up hosts a custom-designed PTFE flow cell with a nominal pathlength of 38 mm and a sample volume of 8 ml. The flow cell is fitted with a custom designed magnetic mixing bar and a miniature glass encapsulated thermistor (Honeywell; calibrated to 0.01°C) that is signal-conditioned and interfaced to the control unit. The light source is provided by three light emitting diodes (LEDs; 435 nm, 494 nm, 596 nm, and 750 nm; Roithner) and light is detected with a spectrophotometer that covers the region between 350 nm and 800 nm with a wavelength resolution of 1.5 nm, a 25 µm slit width, and 14 bits A/D signal conversion (OceanOptics STS VIS-NIR).

2.2. *Principle of the spectrophotometric method*

Hydrogen ion concentration on the total scale (Zeebe and Wolf-Gladrow, 2001) in seawater has been demonstrated to be related to the second dissociation constant (K_2) of an indicator dye (I), the ratio (R) between two absorbance levels produced by the indicator in seawater at the wavelengths corresponding to absorbance maxima of unprotonated (I^{2-}) and monoprotonated (HI^-) forms, and a set of molar absorption ratios (e_i) as a function of temperature (Clayton and Byrne, 1993):

$$\mathrm{pH_T} = \mathrm{p}K_2 + \log\left(\frac{R - e_1}{e_2 - R \cdot e_3}\right) \quad (1a)$$

where $pH_T = -\log[H^+]_T$, $[H^+]_T = [H^+] + [HSO_4]^-$ and $K_2 = [H^+]_T[I^{2-}][HI^-]^{-1}$ (1b)

Suitable indicators, for example *m*-cresol purple and thymol blue, have been characterized in terms of absorbance and proton exchange behaviour (Clayton and Byrne, 1993; Zhang and Byrne, 1996) and extensively used for seawater pH measurements. Such characterizations provide stoichiometric models for the HI^- and I^{2-} forms for a range of salinity and temperatures. The following relationship has been empirically derived for thymol blue for 5 °C ≤ temperature (T) ≤ 35 °C and 30 ≤ salinity (S) ≤ 40 (Zhang and Byrne, 1996):

$$pK_2 = 4.706\ S/T + 26.3300 - 7.17218 \log T - 0.017316\ S \quad (2)$$

where T in equation (2) is in °K. As long as T and S for the sample are measured and a complete set of spectral data relative to the measurement are recorded, the model of the indicator can be refined through post-processing to improve accuracy of the calculated pH. DelValls and Dickson (1998) reported the investigation of pH through high quality e.m.f. measurements of buffers based on 2-amino-2-hydroxymethyl-1,3-propanediol (Tris) in synthetic sea water; based on their recommendation, the pK_2 value of our non-purified thymol blue dye has been adjusted by adding 0.0047 to pH obtained at measurement conditions.

2.3. *Operation*

Prior to a programmed sampling sequence, a set of ancillary data is retrieved from the FerryBox: temperature of the water at the ship's inlet, salinity, time, and coordinates. The light source is switched off and a dark spectrum is acquired with the programmed integration time. Transmission levels may vary during a long term deployment; hence the system adjusts spectral counts at the detector, acting on each of the LED currents, the spectrophotometer integration time, and the number of spectra for averaging (the latter defining the total integration time). In this way the LEDs are kept to the lowest current compatible with a minimum spectrometer's integration time, thus preventing degradation of the LEDs, keeping the spectrophotometer far from saturation and, at the same time, with a suitable signal/noise rejection related to the total integration time.

The water sample to be analysed is introduced into the system, then the water flow is stopped and the system checks that the light levels corresponding to analysis wavelengths are stable; a set of blank (seawater) spectra is acquired and logged, as well as the actual temperature of the sample. A dye solution of 2 mM thymol blue sodium salt (Aldrich) in deionized water (ρ>1 MΩ cm) is pumped into the sample at a mixing ratio of around 0.005 with absorbance at 435 nm around 0.8. The concentration of the dye in the sample + dye solution is proportional to the absorbance (A_{iso}) at the isobestic wavelength of thymol blue (494 nm). The constant of this linear relationship is determined empirically and is proper for the optical pathlength. The change in salinity of the sample can be estimated using the mixing ratio.

After measuring the absorbance of the sample, a sequence of up to four indicator dye addition steps is performed to evaluate the dye perturbation effect on sample pH. These dye perturbation steps measure absorbance levels at higher indicator concentrations and, in general, at different temperatures. All spectral acquisitions are performed when light levels sensed by the spectrophotometer's charge-coupled device (CCD) are stable (mixing and settling time). Temperature drift of the sample is strictly connected to flow cell temperature and thermal isolation. Under normal underway operations, where the cuvette is being continuously

flushed, a maximum drift of 0.02 °C is observed during post injection collection of a single averaged spectrum. Temperature stability of the flow cell is helped by the flushing and pre-equilibration with *in situ* seawater during flushing step of the sampling sequence operation, and this has proven to be crucial for achieving high precision and preventing changes in the light beam geometry due to thermal expansion (around 100 ppm/°C for PTFE). It is worth of remarking that temperature homogeneity of the sample is also very important. Measurements with thermistors on the four sides of the flow cell confirmed that the temperature drift is limited to 0.02 °C and that such drift occurs in a uniform way along the light path.

2.4. *Evaluation of absorbance levels*

Absorbance measured at a specific wavelength (A_λ) of the detection system is defined as:

$$A_\lambda = \log\frac{I_i(\lambda)}{I_o(\lambda)} \quad (3)$$

given light intensities at the input (I_i) and output (I_o) of the flow cell. Strictly, the input intensity refers to the collimated beam emerging from the input window (glass/sample discontinuity) and the output intensity refers to the beam arriving to the output window (sample/glass discontinuity).

Using absorbance measured at three wavelengths for seawater: ${}^{bk}A_{435}$ ${}^{bk}A_{596}$ ${}^{bk}A_{\mathrm{ir}}$, and seawater + dye ${}^{pi}A_{435}$ ${}^{pi}A_{596}$ ${}^{pi}A_{\mathrm{ir}}$, the rigorous method for calculating the absorbance ratio *R* comes from the following equations, where superscripts *bk*, *pi* and, *ir* represent blank, post-injection, and infrared reference, respectively:

$$R = \frac{A_{596}}{A_{435}} = \frac{{}^{pi}A_{596} - {}^{bk}A_{596} - ({}^{pi}A_{\mathrm{ir}} - {}^{bk}A_{\mathrm{ir}})}{{}^{pi}A_{435} - {}^{bk}A_{435} - ({}^{pi}A_{\mathrm{ir}} - {}^{bk}A_{\mathrm{ir}})} \quad (4)$$

If we replace the absorbance with the logarithm:

$$A_{596} = \log\frac{{}^{pi}I_{i,596}}{{}^{pi}I_{o,596}} - \log\frac{{}^{bk}I_{i,596}}{{}^{bk}I_{o,596}} - \log\frac{{}^{pi}I_{i,\mathrm{ir}}}{{}^{pi}I_{o,\mathrm{ir}}} + \log\frac{{}^{bk}I_{i,\mathrm{ir}}}{{}^{bk}I_{o,\mathrm{ir}}} \quad (5)$$

and we consider that the input light intensities are stable, i.e., ${}^{pi}I_{i,\lambda} = {}^{bk}I_{i,\lambda}$, then equation (5) can be written as:

$$A_{596} = \log\frac{{}^{bk}I_{o,596}}{{}^{pi}I_{o,596}} - \log\frac{{}^{bk}I_{o,\mathrm{ir}}}{{}^{pi}I_{o,\mathrm{ir}}} \quad (6a)$$

and likewise:

$$A_{435} = \log\frac{{}^{bk}I_{o,435}}{{}^{pi}I_{o,435}} - \log\frac{{}^{bk}I_{o,\mathrm{ir}}}{{}^{pi}I_{o,\mathrm{ir}}} \quad (6b)$$

Such equations can be taken into the measurement process as good estimates of absorbance when the dominant contribution of fluctuations in the input light intensities are the short term ones; these can be effectively rejected limiting the observation with a proper integration time. Intensities that have been reported so far are those obtained by subtracting the dark spectrum (no input light) from actual spectral counts read by the spectrophotometer during the measurement process, and then corrected for non-linearity of the detector.

2.5. *Infrared correction and dye addition effects*

The infrared absorbance (A_ir) is used to remove the contribution of shifts of spectral counts from the absorbance used to calculate the ratio *R* that are not due to actual indicator absorbance. That is, it should compensate light intensity variation due to misalignment or losses in the optical path, mainly due to handling and repositioning of the cuvette after dye addition when using a benchtop spectrophotometer. In this automated system, the flow cell is the cuvette and it is stationary, so variability caused by repositioning is clearly avoided. Nevertheless, due to imperfect beam collimation and alignment, changes in the refractive index of the medium

can affect beam geometry, and these effects are generally non-uniform across the spectrum (dispersion). The infrared correction is based on the assumption that both HI^- and I^{2-} absorbance are affected in similar way by such shift so that we can refer as a common mode noise signal. Here, the light source entering the flow cell is produced through the combination of independent sources; hence, short term shifts of light levels entering the flow cell are not correlated. In any case, the absorbance at the infrared reference wavelength, far from the peaks, should be only correlated to losses in the sample and has been observed to have an average value around 0.0008. With *R* values above 0.4 this shift would be further inherently rejected from evaluation of pH (based on a ratiometric principle) and accounts to the order of the precision.

Perturbation of sample pH due to dye addition depends on the difference between sample pH and the dye solution, and on the buffering capacity of the sample. In order to correct for pH perturbation due to dye injection, a series of discrete indicator additions is performed for every sample, where pH is calculated using the pK_2 model and molar absorption ratios at different dye concentrations. This approach assumes that the indicator effects are additive, which is reasonable if the additions are small. Final indicator concentration in the flow cell after perturbation experiments is around 25 µM. Using the pH_T (*R*,S,T) model (Byrne et al., 1988), the zero addition pH value is inferred estimating the intercept of the linear fitting of the set of measured pH values as function of A_{ir}.

In order to isolate the dye addition effect *in situ*, the system first reports all pH evaluations to the same temperature, which is the average of the temperatures recorded during additions. Surface seawater pH is strongly anti-correlated to temperature and a linear temperature dependence can be approximated (e.g., mean: -0.0155 ± 0.02 K^{-1} over 10 K for five sets of dissociation constants; Millero, 2007). The zero addition intercept has been estimated with a linear regression for each set of measurements, and the root mean square deviation provides the inherent precision for that pH measurement.

2.6. *Laboratory-based tests of system performance*

A series of laboratory-based development was conducted using Tris seawater buffers and CO_2 certified reference material (CRM) (both acquired from Andrew Dickson, Scripps Institution of Oceanography, La Jolla, California, USA). In order to assess analytical uncertainty of the pH measurements, Tris seawater buffers (batch 26) and the same indicator dye batch were measured in succession using the sample analysis steps described in the operations, evaluation, and correction (sections 2.3-2.5). For the Tris seawater buffer evaluation, two identical systems were tested using a total of 28 measurements – in the laboratory in March 2015 (n=8) with system A, and in June 2015 (n=8) and at a field station in Kings Bay, Svalbard in July 2015 (n=12) with system B. The Tris seawater buffer measurements were made at different temperatures but normalized to 25 °C using equilibrium equations implemented by CO2SYS (Pierrot et al., 2006) and certified AT and CT values, and standard deviation of each set of measurements were calculated.

As both a test of the dye perturbation assessment and to provide a secondary assessment of uncertainty, CO_2 certified reference materials (batch 143) were measured in succession using the same sample analysis steps. Using measured pH and certified AT and CT values, an overdetermination of the carbonate system was executed to test the consistency of the measured pH. For the overdetermination, dissociation constants for carbonic acid K_1 and K_2 (Lueker et al., 2000) and boric acid K_B (Lee et al., 2010) were used in conjunction with CO2SYS

(Pierrot et al., 2006). The replicate measurement of batch CRMs were also used to calculate standard deviation as a secondary assessment of measurement uncertainty.

2.7. *Field observations on SOOP MS* Trollfjord

The spectrophotometric pH system operated autonomously alongside a standard FerryBox system (Volent et al., 2011) on the passenger ship MS *Trollfjord* which operates along the Norwegian coast over five time periods in 2015: 28 February - 6 March, 20 April - 24 April, 5 May - 11 May, 18 June - 24 June, and 21 July - 26 July. Each period was of 5-6 days in duration and roughly covered a transect ~4500 km in length along the western coast of Norway from Bergen, Norway (~60 °N) to Kirkenes, Norway (~71 °N). The FerryBox system was flushed and sensors were inspected and cleaned on a monthly basis.

During the sampling periods, the pH system measured seawater pH approximately every five minutes – this included dye pH perturbation experiments on each sample and a timing routine that provided adequate spatial resolution for efficient use of indicator dye. Log files with dye perturbation and temperature-corrected pH were merged with log files containing core FerryBox data that included temperature and salinity (SBE45 and SBE38, Sea-Bird Electronics), and chlorophyll fluorescence (microFlu-chlorophyll, TriOS). Temperature and salinity measurements were periodically checked using secondary calibrated temperature probes and discrete salinity samples for laboratory analysis, respsectively. Chlorophyll a concentrations (μg L^{-1}) were estimated using chlorophyll a fluorescence calibration slopes generated with phytoplankton cultures of known chlorophyll a concentration. Chlorophyll fluorescence data was not available during the 28 February – 6 March time period.

Quality control of the data was performed using multiple routines that flagged data when the ship was performing docking and other logistics-related manoeuvring (the ship makes 34 stops along the Norwegian coast during each transect), when one or more sensors and their system controls were not functioning properly, and/or when seawater temperature at multiple points in the FerryBox system exhibited large variability (>2 °C). The latter is indicative of the FerryBox pump either being switched off or the presence of an obstruction in the system. Data were often flagged at the beginning of each transect due to the ship being stationary at port for an extended period of time (>12 h), and extra flushing of the system was required before normal sensor operation. In order to assess spatial and seasonal variation in the Norwegian Coastal Current, observations presented here are limited to water masses with salinity >29 (Mork, 1981). Due to the range of salinity and temperature for which pK_2 of thymol blue have been determined (Zhang and Byrne, 1996), uncertainties for pH observations at salinity <30 and temperature <5 °C may be slightly greater than the estimated *in situ* uncertainty and will be evaluated in a future study.

3. Results and Discussion

3.1. Lab-based assessment using Tris seawater buffers and CO_2 certified reference material

Twenty-eight pH measurements of various bottles of Tris seawater buffers (Dickson laboratory, batch 26) were made using two different systems that were built to identical specification (Fig. 2). The dye perturbation experiments revealed that, as expected, the buffering capacity of the Tris buffer was sufficient enough that indicator addition did not perturb pH. Within a measurement temperature range of 0.02 ºC the variability observed on pH was typically <0.0005. The measurements were normalized to 25 °C using the slope of the linear regression between pH and measurement temperature (Fig. 3), and the resulting standard deviation

of measurements made by the two separate systems was ~0.0004. Taking into account the 0.002 uncertainty in pH that was assigned to the prepared Tris seawater buffer, the combined additive uncertainty was <0.0024. This uncertainty meets the "weather" and "climate" objectives of 0.02 and 0.003 in pH, respectively, as determined by the Global Ocean Acidification Observing Network (Newton et al., 2015).

The pH measurements performed on the CO_2 CRMs (batch 143) are shown in Fig. 4. Here, the effect of dye addition was evident through the ~0.0010-0.0015 decrease in pH per step of dye addition. Using the pH measurement, the certified AT value (2241.04 µmol kg^{-1}), and CO2SYS, the sample pH values at 25 °C can be calculated and resulting mean and standard deviation of these measurements is 7.9247 ± 0.0006. This uncertainty agrees well with the uncertainty of the Tris seawater buffers measurements of 0.0004. The pH measurements on the CO_2 CRMs were further used to perform an overdetermination analysis of the carbonate system (Table 1). The uncertainty of the CO2SYS-calculated AT and CT values are <0.3 µmol kg^{-1} and are within the uncertainty reported for state-of-the-art techniques used to make certified values that accompany the CRMs (Dickson et al., 2007).

Despite these laboratory-based tests, the accuracy of the system is largely dominated by uncertainties associated with dye dissociation constants and dye addition (Bellerby et. al, 2002), and therefore by the uncertainty resulting from the estimate of the linear fitting in Fig. 4. The uncertainty from the coefficient used to report the pH to the same temperature, $\delta(\partial \mathrm{pH}/\partial \mathrm{T})$, accounts for pH uncertainty as a function of temperature. During the dye addition sequence, temperature may vary up to ±0.5 ºC and the residual uncertainty is on the order of precision of 0.0005. The system achieves the estimate of the slope of the pH(A_{iso}) linear fitting to better than 0.002. With an average 0.4 isobestic absorbance, the residual uncertainty on pH is <0.001. Combined with uncertainty of 0.002 on the p*K* for thymol blue (Zhang and Byrne, 1996), the combined uncertainty is the root mean square of the three uncertainties which is ~0.0029, which is comparable with estimated uncertainty of 0.0024 acquired from the measurements with the Tris seawater buffer.

Combining the measurement uncertainty, the uncertainty of the temperature coefficient of pH, and the uncertainties for *in situ* and measured temperature (respectively, at the inlet of the FerryBox system and inside the flow cell), the resulting uncertainty introduced by calculation at *in situ* conditions can be written as:

$$\delta(\mathrm{pH})_{\mathrm{is}} = \sqrt{[\delta(\mathrm{pH})_{\mathrm{m}}]^2 + \left[\delta\left(\frac{\partial \mathrm{pH}}{\partial \mathrm{T}}\right) \cdot (\mathrm{T_m} - \mathrm{T_{is}})\right]^2 + [0.016 \cdot (\delta \mathrm{T_m} + \delta \mathrm{T_{is}})]^2} \,. \quad (7)$$

Considering that the difference T_m-T_{is}, during normal operations is limited to 1.5 ºC and $\delta T_m \approx \delta T_{is} \approx 0.02$ ºC, from a base uncertainty of 0.0024 it follows that the FerryBox-coupled spectrophotometric pH detection system can determine *in situ* pH with uncertainty of <0.003.

3.2. Field-collected pH measurements between February-July 2015 along the Norwegian Coast

Data collected by the FerryBox and pH systems on the M/S *Trollfjord* along the Norwegian Coastal Current between February and July 2015 exhibited large seasonal and regional variability in temperature, salinity, chlorophyll a (as estimated from fluorescence), and pH. The major observed changes from winter to spring to summer include: (1) a ~4-9 °C warming with wintertime minimum of 2 °C near Kirkenes and summertime maxima of ~13 °C along many parts of the coast south of 70 °N and especially near Kristiansund and the Lofoten Islands (62 °N and 68 °N); (2) Salinity in winter was relatively stable(mean = 33.2 ± 0.6) while

summertime salinity was lower and more variable (July mean = 32.6 ± 1.6), especially near Måløy, Kristiansund, and Trondheim (62-63.5 °N), and near Sandnessjøen (~66 °N); (3) Chlorophyll a maxima were observed in April above ~68 °N with chlorophyll a concentrations reaching 10 µg L^{-1}, while moderate chlorophyll a concentrations up to ~3 µg L^{-1} were present throughout region in spring and summer, especially north of 70 °N; and (4) Generally lower pH and lower variability during winter (Feb/Mar 2015 mean = 8.051 ± 0.014) and higher pH and higher variability (2.2 to 3.6-fold higher) in spring and summer (April 2015 mean = 8.138 ± 0.051 ; May 2015 mean = 8.150 ± 0.033; June 2015 mean = 8.151 ± 0.035; July 2015 mean = 8.148 ± 0.031).

Southern Norway tended to be lower in pH druing the spring and summer months, especially near the opening of the Trondheimsfjord where pH remained <8.080 throughout the study period, and between Måløy and Ålesund (~62-62.5 °N) with a number of observations <8.100 in spring and early summer. Regional maxima in pH were quite variable in terms of location and timing, but some pH values as high as 8.247 were observed near Bodø (67 °N) in April, June, and July, as high as 8.295 in the vicinity of the Lofoten Islands (~68 °N) in April and June, as high as 8.272 near Tromsø (70 °N) in April, May, and June, and as high as 8.246 near Kirkenes (70 °N) in May and June. Despite the general relationship between primary production using CO_2 and therefore increasing pH, there was no significant correlation between high chlorophyll a and high pH observations. Similarly, although there were coinciding observations of low salinity and generally lower pH along southern Norway in the spring and summer periods, there was no region-wide correlation between the two variables. This may have been due to water mass heterogeneity forced by large influences of physical processes on pH such as warming, freshwater input, ocean-atmosphere interactions, and or mixing.

To put these observations in perspective, the average ~0.1 increase in pH which was observed between February/March and the spring/summer months, assuming a constant AT typical for the Norwegian Coastal Current (2310 µmol kg^{-1}) and no change in temperature, would result in ~80 ppm lower partial pressure of CO_2 (pCO_2) (Pierrot et al., 2006). The largest winter to summer change in pH occurred near the Lofoten Islands with a ~0.255 increase in pH. Again, assuming a constant AT and temperature, this increase in pH would result in ~170 ppm lower pCO_2. The magnitude of the observed seasonal variability in the carbonate system is large relative to projected decadal scale change (e.g., mean ocean pH by ~2040 is projected to decrease by 0.1 in a business as usual scenario; IPCC, 2013). It is therefore important to take seasonal and regional variability in pH and pCO_2 into account when evaluating the projected decadal and century scale changes in the carbonate system – most notably the rise in CO_2 and decline in pH due to fossil fuel CO_2 emissions.

4. CONCLUSIONS

Here we have shown that an autonomous pH measurement system capable of theoretical and operational uncertainties of <0.003. This has been tested using Tris seawater buffers and seawater CO_2 CRMs with multiple units built to identical specifications. The system has also been deployed on a SOOP covering >4000 km along the Norwegian coast for a winter-summer observation period. The data reveals hotspots in the Norwegian Coastal Current where there are minima, maxima, and/or high seasonal variability in environmental drivers like temperature, salinity, and pH. Future work will focus on implementing sensors that can provide a second carbonate chemistry variable (e.g., pCO_2, AT, CO_3^{2-}) to enable a full characterization of the carbonate system. The embedded flow-through spectrophotometry set-up that has been used for the present pH system has been also considered for direct measurement of CO_3^{2-} ions concentration (Easley et al., 2013) as well as for AT

(Spaulding et al., 2014). For seawater pCO_2, several equilibrator-style and spectrophotometric systems are currently commercially available.

Spectrophotometry combined with embedded systems has been illustrated in this work as the ideal tool for high resolution surface pH survey of coastal environments when supported by FerryBox equipped SOOP. Analytical uncertainties are comparable to the best laboratory analytical techniques and "climate" quality goals are achievable by an autonomous system over extended periods. The operation and integration with other monitoring systems like a FerryBox flow-through system can improve our capability in measuring carbonate chemistry variability and ecosystem response to OA, with the eventual goal of better understanding carbonate system variability in surface coastal waters, contributing to the refinement of biogeochemical models of continental shelf processes, and investigating variability in biogeochemical processes driven by natural and anthropogenic stressors.

ACKNOWLEDGEMENTS

This research has been funded by the EU FP7 JERICO project (Joint European Research Infrastructure network for Coastal Observatories, EU FP7-262584), the Centre for Environment-friendly Energy Research (FME) SUCCESS (SUbsurface CO_2 storage – Critical Elements and Superior Strategy), the Fram Centre flagship on Ocean Acidification (Current OA state and variability – OA-STATE), and NIVA's Strategic Research Initiative on Ocean Acidification (OASIS). A sincere credit goes to I. Becsan (NIVA) for his support in fabrication, installation, and testing of mechanical parts, and J. Dedric Berg (NIVA) for the follow-up on IP issues and S. Tveite (WAG Solutions) on commercial issues. Two anonymous reviewers also provided valuable comments that improved the manuscript. The FerryBox line mentioned in this work are part of NIVA SOOP network that started in 2001 for water quality, operational oceanography, and satellite product validation, and the network is also supported by the Norwegian Ocean Acidification survey (Monitoring Ocean Acidification in Norwegian Waters, Norwegian Environmental Agency) and the Coastal Monitoring Program for Eutrophication (Water Framework Directive; Norwegian Environmental Agency ØKOKYST program).

REFERENCES

Aßmann, S., Frank, C. , Körtzinger, A., "Spectrophotometric high-precision seawater pH determination for use in underway measuring systems", Ocean Sci. Discuss., 2011, 8:1339–1367

Bellerby, R. G. J, Olsen, A., Johannessen, T., Croot, P., "A high precision spectrophotometric method for on-line shipboard seawater pH measurements: the automated marine pH sensor (AMpS)",Talanta, 2002, 56(1):61-69.

Byrne, R. H., Robert-Baldo, G., Thompson, S. W., Chen, C. T. A., "Seawater pH measurements: an at-sea comparison of spectrophotometric and potentiometric methods", Deep-sea Res., 1988, A 35(8): 1405–1410.

Clayton, T. D., and Byrne, R. H., "Spectrophotometric seawater pH measurements: total hydrogen ion concentration scale calibration of *m*-cresol purple and at-sea results", Deep-Sea Res. 1993, A 40(10):2115-2129

Dickson, A.G., Sabine, C.L. and Christian, J.R. (Eds.), Guide to best practices for ocean CO_2 measurements, 2007.

Doney, S. C., Fabry V. J., Feely R. A., and Kleypas, J. A., "Ocean Acidification: The Other CO_2 Problem", Annu. Rev. Mar. Sci., 2009, 1:169-192

DelValls, T. A., Dickson, A. G., "The pH of buffers based on 2-amino-2-hydroxymethil-1,3-propanediol('tris') in synthetic seawater", Deep-Sea Res. I, 1998, 45:1541-1554

DelValls, T.A., “Underway pH measurements in upwelling conditions: The California Current”, Cien. Mar., 1999, 25:345-365

Easley R. A., Patsavas, M. C., Byrne, R. H., Liu, X., Feely, R. A., Mathis, J. T., “Spectrophotometric Measurement of Calcium Carbonate Saturation States in Seawater”, Environ. Sci. Technol., 2013, 47 (3): 1468-1477

Hofmann, G. E., Smith, J. E., Johnson, K. S., Send, U., Levin, L. A., Micheli, F., Paytan, A., Price, N. N., Peterson, B., Takeshita, Y., Matson, P. G., Crook, E. D., Kroeker, K. J., Gambi, M. C., Rivest, E. B., Frieder, C. A., Yu, P. C., and Martz, T. R., “High-frequency dynamics of ocean pH: A multi-ecosystem comparison”, PLoS ONE, 2011, 6, e28983, doi:10.1371/journal.pone.0028983

IPCC: Climate Change 2013: The Physical Science Basis. Contribution of Working Group I to the Fifth Assessment Report of the Intergovernmental Panel on Climate Change [Stocker, T.F., D. Qin, G.-K. Plattner, M. Tignor, S.K. Allen, J. Boschung, A. Nauels, Y. Xia, V. Bex and P.M. Midgley (eds.)]. Cambridge University Press, Cambridge, 2013, United Kingdom and New York, NY, USA, 1535 pp, doi:10.1017/CBO9781107415324

Kaltenbacher, E., Steimle, E., Byrne, R., “A compact, in-situ, spectrophotometric sensor for aqueous environments: design and applications”, IEEE, 2000, 41–45

Lee, K., Kim, T.W., Byrne, R.H., Millero, F.J., Feely, R.A., Liu, Y.M., “The universal ratio of boron to chlorinity for the North Pacific and North Atlantic oceans”, Geochim.Cosmochim. Acta, 2010, 74 (6), 1801–1811

Liu, X., Wang, W.A., Byrne, R.H., Kaltenbacher, E.A., Bernstein, R.E. “Spectrophotometric measurements of pH in-situ: laboratory and field evaluations of instrumental performance”, Environ. Sci. Technol., 2006, 40: 5036–5044

Lueker, T.J., Dickson, A.G., Keeling, C.D., “Ocean pCO_2 calculated from dissolved inorganic carbon, alkalinity, and equations for K_1 and K_2 : validation based on laboratory measurements of CO_2 in gas and seawater at equilibrium”, Mar. Chem., 2000, 70 (1-3): 105–119

Martz, T.R., Carr, J.J., French, C.R., DeGrandpre, M.D., “A submersible autonomous sensor for spectrophotometric pH measurements of natural waters”, Anal. Chem., 2003, 75: 1844–1850

Martz, T.R., Daly, K.L., Byrne, R.H.,Stillman, J.H., and Turk, D., “ Technology for Ocean Acidification Research: Needs and Availability”, Oceanography, 2015, 28(2):40-47.

McNeil, B.I., Sasse, T.P, “Future ocean hypercapnia driven by anthropogenic amplification of the natural CO2 cycle”, Nature, 2016, 529:383-386

Millero, F.J., “The Marine Inorganic Carbon Cycle”, Chem. Rev., 2007, 107: 308-341

Mork, M., "Circulation Phenomena and Frontal Dynamics of the Norwegian Coastal Current". Philosophical Transactions of the Royal Society A: Mathematical, Physical and Engineering Sciences, 1981, 302(1472): 635

Mosley, L.M., Husheer, S.L.G., Hunter, K.A., “Spectrophotometric Calibration of pH Electrodes in Seawater Using Purified m-Cresol Purple”, Mar. Chem., 2004, 91:175–186

Nakano, Y., Kimoto, H., Watanabe, S., Harada, K., Watanabe, Y.W., “Simultaneous measurements of in situ pH and CO_2 in the sea using spectrophotometric profilers”, J. Oceanogr., 2006, 62: 71–81

Newton, J. A., Feely, R. A., Jewett, E. B., Williamson, P., Mathis, J., Global Ocean Acidification Observing Network: requirements and governance plan, 2014.

Ohline, S.M., Reid, M.R, Husheer, S.L.G., Currie, K.I., Hunter, K.A., “Spectrophotometric determination of pH in seawater off Taiaroa Head, Otago, New Zealand: Full-spectrum modeling and prediction of pCO2 levels”, Mar. Chem., 2007, 107: 143–155

Petersen, W., “FerryBox systems: state-of-the-art in Europe and future development”, J. Mar. Sys., 2014, 140A:4-12

Pierrot, D. E. Lewis, D. W. R. Wallace. 2006. MS Excel Program Developed for CO2 System Calculations. ORNL/CDIAC-105a. Carbon Dioxide Information Analysis Center, Oak Ridge National Laboratory, U.S. Department of Energy, Oak Ridge, Tennessee

Reggiani, E. R., Bellerby, R. G. J., Sørensen, K., “Underwater spectrophotometric detection: scaling down ocean acidification monitoring”, 2014, Sensor Systems for a Changing Ocean, 1-5

Rérolle, V.M.C., Floquet, C.F.A., Harris, A.J.K., Mowlem, M.C., Bellerby, R.G.J., Achterberg E.P., “Development of a colorimetric microfluidic pH sensor for autonomous seawater measurements”, Anal. Chim. Acta, 2013, 786: 124-131

Sabine, C.L., Feely, R.A., Gruber, N., Key, R.M., Lee, K., Bullister, J.L., Wanninkhof, R., Wong, C.S., Wallace, D.W.R., Tilbrook, B., Millero, F.J., Peng, T.-H., Kozyr, A., Ono, T., and Rios, A. F, “The oceanic sink for anthropogenic CO_2”, Science, 2004, 305: 367–371

Seidel, M.P., DeGrandpre, M.D., Dickson, A.G., “A sensor for in situ indicator-based measurements of seawater pH”, Mar. Chem., 2008, 109: 18–28

Spaulding, R.S., DeGrandpre, M.D., Beck, J.C., Hart, R.D., Peterson, B., De Carlo, E.H., Drupp., P.S., and Hammar T.R., “Autonomous in situ measurements of seawater alkalinity”, Environ. Sci. Technol., 2014, 48: 9573-9581

Tapp, M., K. Hunter,K., Currie, K., Macaskill, B., “Apparatus for continuous-flow underway spectrophotometric measurement of surface water pH”, Mar. Chem., 2000, 72: 193–202

Volent, Z., Johnsen, G., Hovland, E.K., Folkestad, A, Olsen, L.M., Tangen, K., Sørensen, K., “Improved monitoring of phytoplankton bloom dynamics in a Norwegian fjord by integrating satellite data, pigment analysis, and Ferrybox data with a coastal observation network”, J. Appl. Remote Sens., 2011, 5(1):053561, doi:10.1117/1.3658032

Wang, Z.A., Liu, X., Byrne, R.H., Wanninkhof, R., Bernstein, R.E, Kaltenbacher, E.A., Patten, J., “Simultaneous spectrophotometric flow-through measurements of pH, carbon dioxide fugacity, and total inorganic carbon in seawater”, Anal. Chim. Acta, 2007, 596: 23–36

Wang., Z.A., Sonnichsen, F.N., Bradley, A.M., Hoering, K.A., Lanagan, T.M., Chu, S.N., Hammar, T.R. and Camilli, R., “In situ sensor technology for simultaneous spectrophotometric measurements of seawater total dissolved inorganic carbon and pH”, Environ. Sci. Technol., 2015, 49, 4441-4449.

Yang, B., Patsavas, M.C., Byrne, R.H., Ma, J., “Seawater pH measurements in the field: A DIY photometer with 0.01 unit pH accuracy”, Mar. Chem., 2014, 160: 75-81

Zeebe, R. E., Wolf-Gladrow, D., in CO_2 in seawater: equilibrium, kinetics, isotopes, 2001, 65.

Zhang, H., and Byrne, R. H., “Spectrophotometric pH measurements of surface seawater at in-situ conditions: absorbance and protonation behavior of thymol blue”, Mar. Chem., 1996, 52: 17–25

FIGURE CAPTIONS

Figure 1. Schematic of the pH sampling and detection system. (a) light emitting diode light source, (b) power combiner, (c) input optical fiber, (d) output valve, (e) input valve, (f) bypass valve, (g) dye injection port, (h) temperature probe, (i) output optical fibre, (j) spectrophotometer, (k) interface and control unit.

Figure 2. Measurements of pH (total scale) of Tris seawater buffer (batch 26) at various flow cell temperatures (°C) based three measurements periods: March 2015 in the laboratory with system A, slope = 0.0310 pH $°C^{-1}$, n=8 (○), June 2015 in the laboratory with system B, slope = 0.0308 pH $°C^{-1}$, n=8 (∇), and July 2015 at a field station with system B, slope = 0.0308 pH $°C^{-1}$, n=12 (□). Error bars represent 1 standard deviation calculated using each set of measurements.

Figure 3. Differences between measured pH (total scale) of Tris seawater buffer shown in Fig. 2 normalized to 25 °C (n=28) and the assigned pH of the Tris seawater buffer (8.0935). Error bars represent 1 standard deviation calculated using each set of measurements. Dashed lines at ±0.002 represent the assigned uncertainty of the Tris seawater buffer.

Figure 4. Two sample runs showing the relationship between isobestic absorption (A_{iso}) and pH of CO_2 certified seawater reference material after four indicator dye perturbations. pH (total scale) is reported at the average flow cell temperature (°C) during the analysis cycle. The dye perturbation-corrected pH of Batch 143 #1 (B143) is 7.9421 at 23.84 °C (○), and of B143 #2 is 7.9310 at 24.55°C (∇). Error bars represent 1 standard deviation of calculated using each set of measurements.

Figure 5. Transect data of Norwegian Coastal Current mixed layer waters including temperature (°C), salinity, chlorophyll a estimated from fluorescence (µg L^{-1}; note that data are plotted on a log scale), and pH (total scale) for the time periods of: a) 28 February - 6 March 2015, b) 20 April - 24 April 2015, c) 5 May - 11 May 2015, d) 18 June - 24 June 2015, and e) 21 July - 26 July 2015. Color bars for each variable are shown on the same scale regardless of month for visual clarity. Major landmarks are denoted on the top figure of panel a) as Kirkenes (Ki), Tromsø (T), Lofoten Islands (L), Bodø (Bo), Sandnessjøen (S), Trondheim (T), Kristiansund (Kr), and Bergen (Be). Chlorophyll a fluorescence data were not available for the 28 February - 6 March 2015 period.

TABLES

Table 1. Two pH measurements including correction of dye perturbation effects using CO_2 certified reference material from Batch 143. pH (total scale; pH_T) is reported at the temperature in the flow cell during sample analysis (T_{ref}, °C), and also normalized to 25 °C using CO2SYS and certified total alkalinity (AT; µmol kg^{-1}). The results of the overdetermination are shown in the calculated total DIC (CT; µmol kg^{-1}) and AT columns. CT values were calculated using CRM AT, salinity, phosphate, silicic acid, T_{ref}, and pH_T. AT values were calculated using CRM CT, salinity, phosphate, silicic acid, T_{ref}, and pH_T. 1 standard deviation of the calculated CT and AT values is 0.21 and 0.28 µmol kg^{-1}, respectively.

				certified		calculated	
B143	pH_T	T_{ref}	pH_{T25}	CT	AT	CT	AT
#1	7.9421	23.84	7.9249	2017.75	2241.04	2017.50	2241.40
#2	7.9310	24.55	7.9244	2017.75	2241.04	2017.80	2241.00

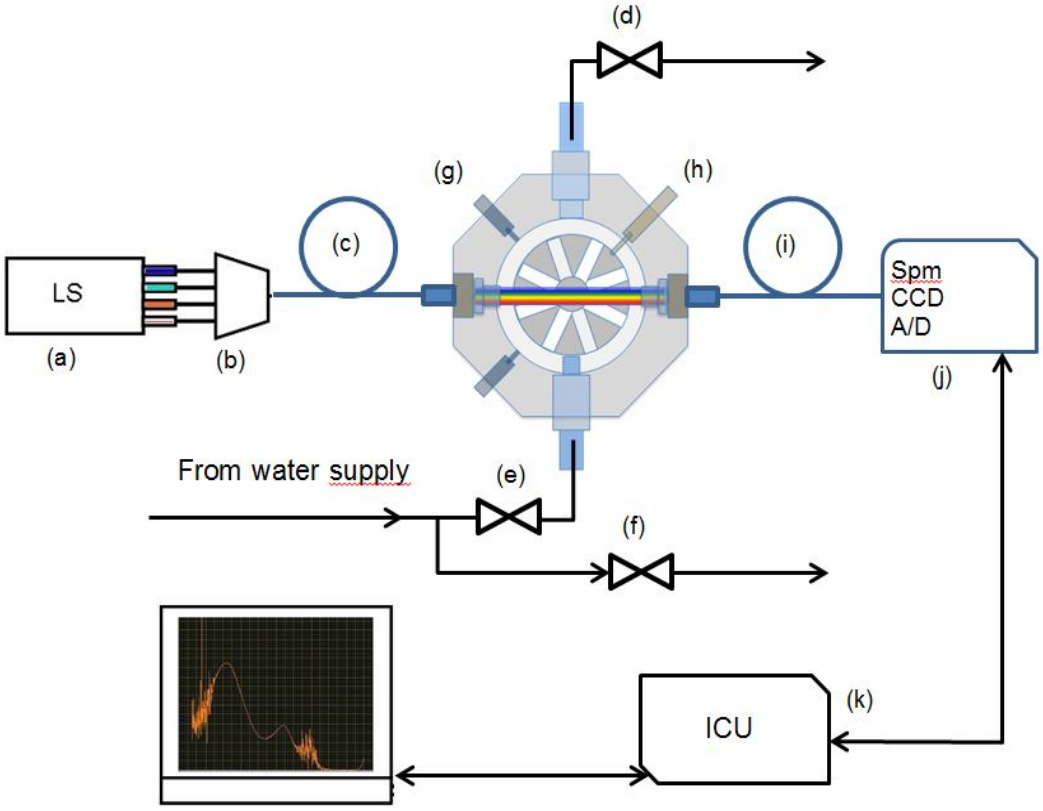

Figure 1

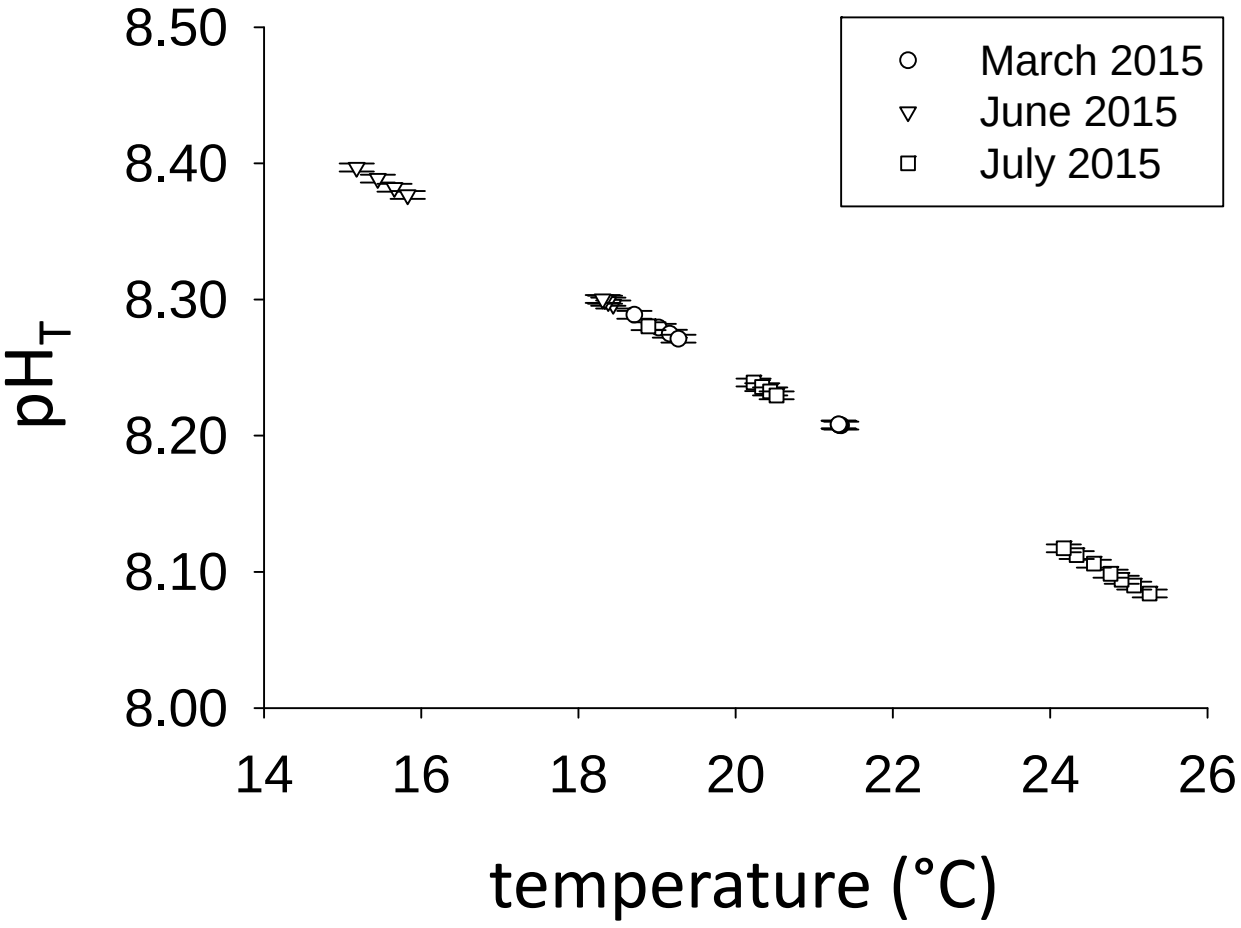
8.50
8.40
8.30
8.20
8.10
8.00
pH$_T$
14
16
18
20
22
24
26
temperature (°C)
March 2015
June 2015
July 2015

Figure 2

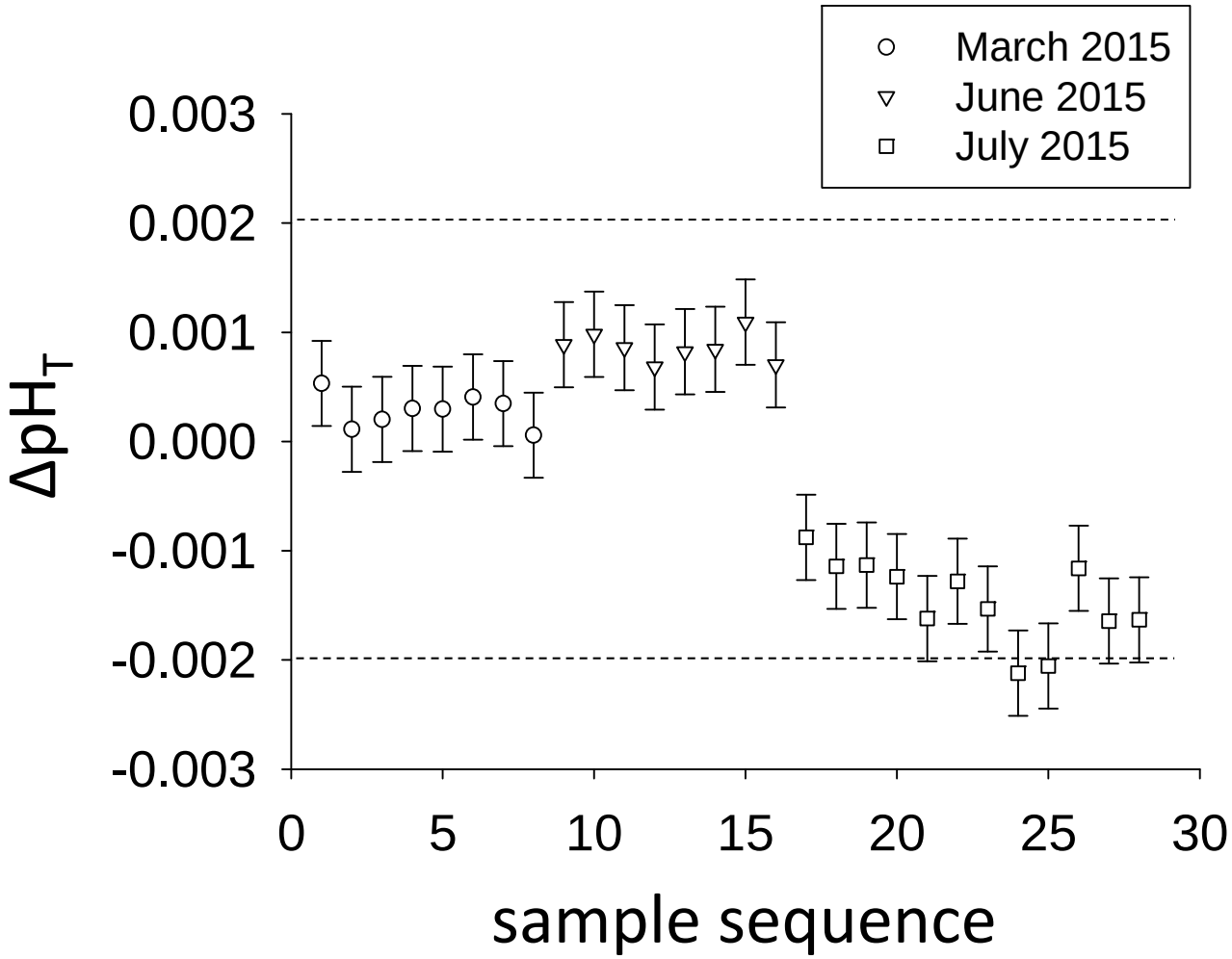
March 2015
June 2015
July 2015
0.003
0.002
0.001
0.000
-0.001
-0.002
-0.003
ΔpH_T
0
5
10
15
20
25
30
sample sequence

Figure 3

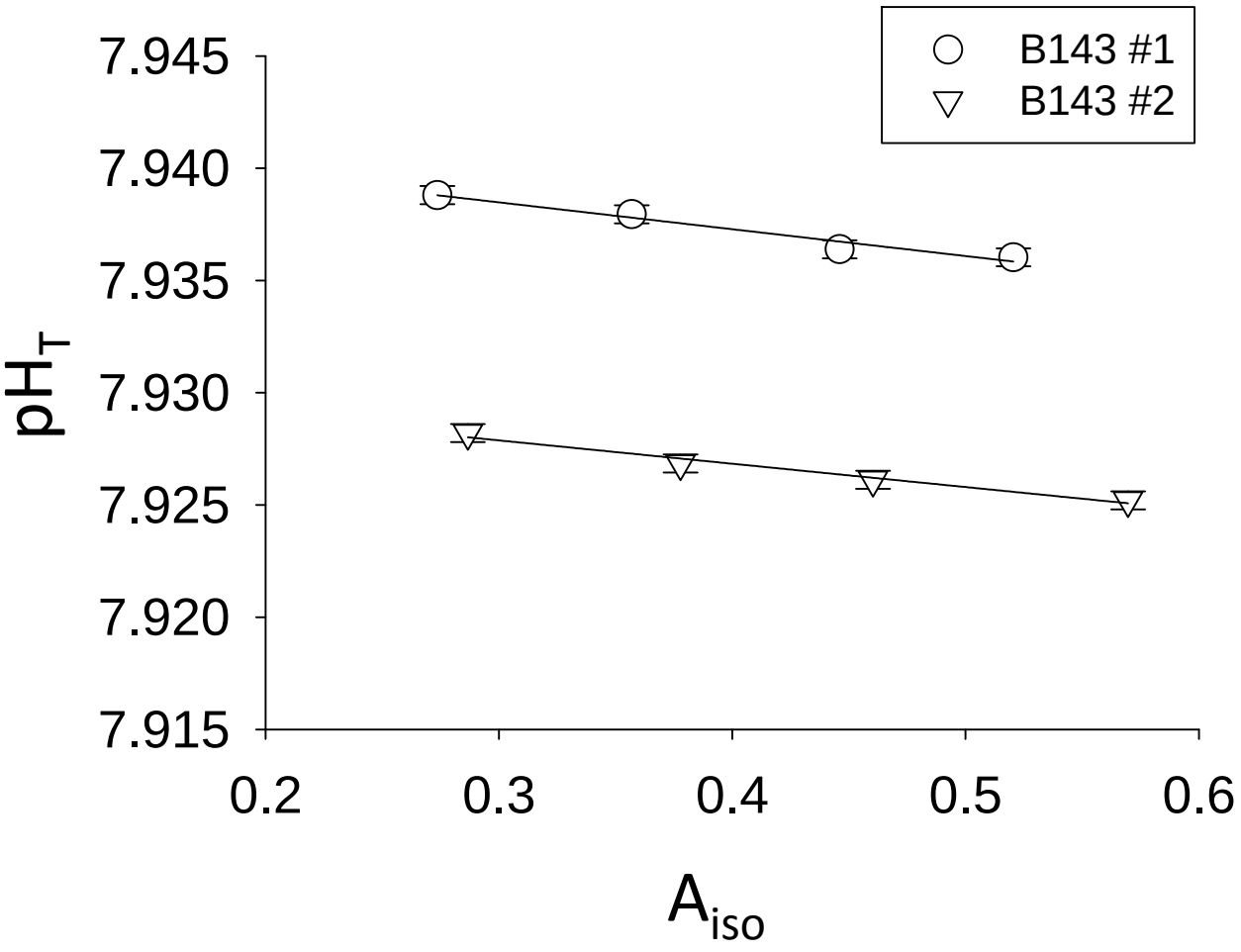
B143 #1
B143 #2
7.945
7.940
7.935
7.930
7.925
7.920
7.915
pH_T
0.2
0.3
0.4
0.5
0.6
A_iso

Figure 4

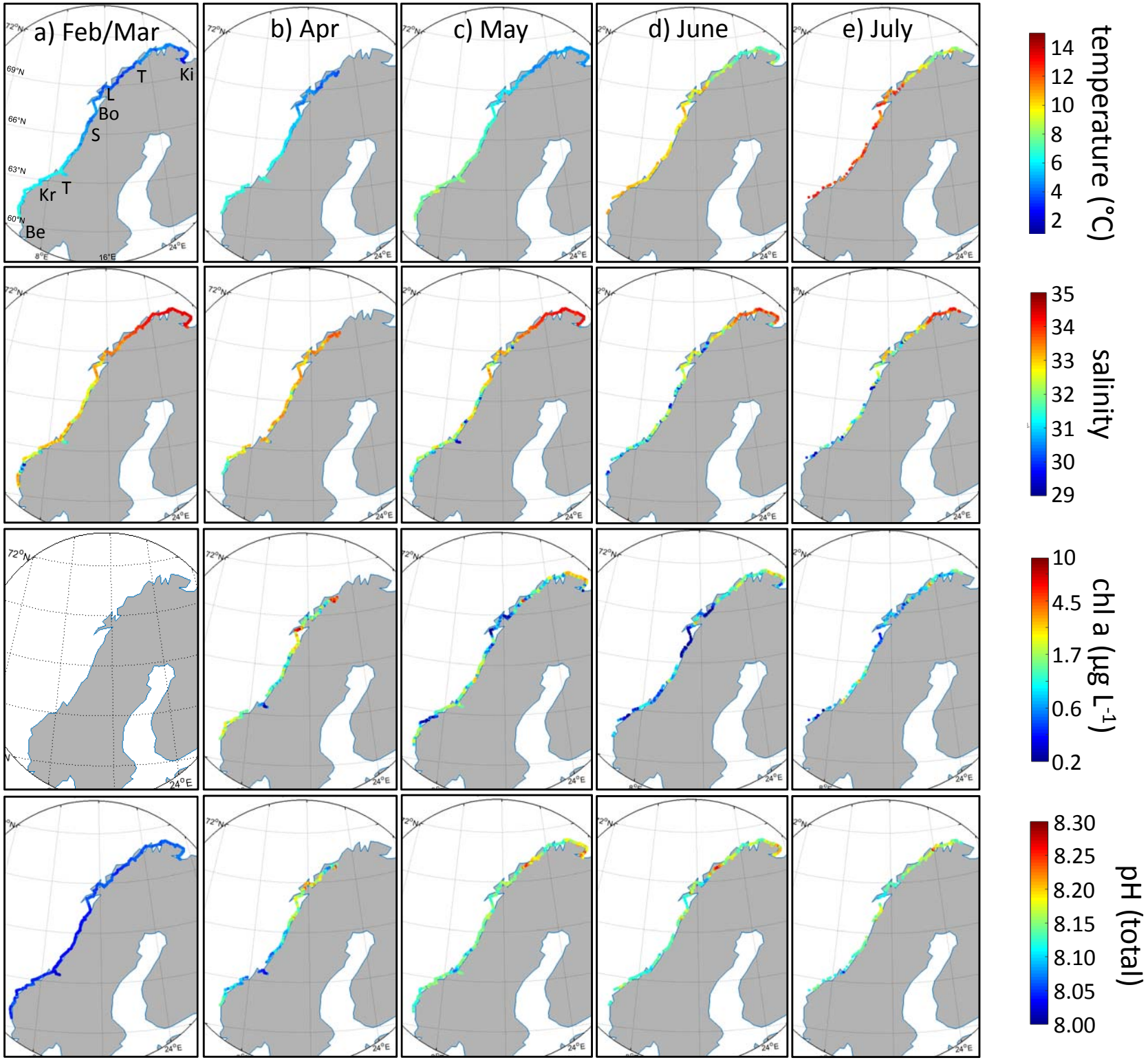
a) Feb/Mar
b) Apr
c) May
d) June
e) July
Ki
T
L
Bo
S
Kr
T
Be
temperature (°C)
14
12
10
8
6
4
2
salinity
35
34
33
32
31
30
29
chl a (µg L-1)
10
4.5
1.7
0.6
0.2
pH (total)
8.30
8.25
8.20
8.15
8.10
8.05
8.00

Figure 5